

BME MSc Thesis
(BM51035)

Collagen Turnover Modeling in a Rapid Zero-Dimensional Growth Framework:

Toward Efficient Simulation
of Post-Infarct Remodeling

A. Tuttolomondo

Collagen Turnover Modeling in a Rapid 0D Growth Framework

Toward Efficient Simulation of Post-Infarct Remodeling

By

Alessandro Tuttolomondo

In partial fulfilment of the requirements for the degree of:

Master of Science
in Biomedical Engineering

at the **Delft University of Technology**,
to be defended publicly on Friday June 13, 2025 at 8:45 AM.

Supervisor: dr. ir. Mathias Peirlinck, Ludovica Maga

Thesis committee:

dr. ir. Mathias Peirlinck	TU Delft
Dr. Selene Pirola	TU Delft
Daniel Verhülsdonk	TU Delft

Content

1. Introduction

- 1.1 Relevance
- 1.2 Motivation & Research Goal

2. Methodology

- 2.1 Circulation Framework
- 2.2 Growth Simulation
- 2.3 Tuning Baseline and Acute Hemodynamics
- 2.4 Collagen Turnover Modeling

- 2.5 Verification and Validation

3. Results

- 3.1 Model Verification
- 3.2 CT Function Optimization
- 3.3 Model Validation

4. Discussion

- 4.1 Prediction Accuracy
- 4.2 Modeling CT
- 4.3 Limitations
 - 4.3.1 Early Discrepancies: Tuning Baseline Input Parameters
 - 4.3.2 Spatial Characterization
 - 4.3.3 Phenomenological Simplifications

5. Future Outlook

6. Conclusion

Appendices

- A.1 List of Abbreviations
- A.2 Input Parameters
- A.3 Geometry
 - A.3.1 Compartmental Parameters Scaling
 - A.3.2 Thin-Walled Sphere Geometry and Mechanics
- A.4 Z-Score Based Optimization for Stiffness Law Calibration
- A.5 Collagen Turnover: Alternative Sigmoidal Formulation
- A.6 Joint Optimization of V_0 and V_{wall} for Geometric Consistency

Acknowledgments

This Master's thesis represents a significant milestone in my academic journey and marks a key step toward my professional career.

First and foremost, I would like to express my sincere gratitude to my thesis supervisor, Dr. ir. Mathias Peirlinck, and my daily supervisor, Ludovica Maga, for their invaluable guidance, encouragement, and critical insights throughout this work. Their mentorship has profoundly shaped my scientific mindset and approach to modeling, consistently challenging me to grow beyond my perceived limits.

I would also like to thank the Department of Biomechanical Engineering at TU Delft and all members of the PeirlinckLAB group for fostering a stimulating environment of intellectual exchange and continuous support.

I am grateful to all the people who, at various stages, accompanied me on this journey in the Netherlands. Thank you for your support, inspiration, and contributions to both my academic and personal development.

My deepest appreciation goes to my lifelong friends from Pergo. You have always felt like a second family, and I share this achievement with you.

A special thanks goes to Martina. Your unwavering love and support made this possible. Thank you for standing by my side each day and encouraging me to strive for excellence.

Lastly, I dedicate this work entirely to my family. I am deeply thankful to have you in my life. Your belief in me and constant encouragement have always been my greatest motivation to grow into a better person.

Thank you,

Alessandro

Collagen Turnover Modeling in a Rapid 0D Growth Framework: Toward Efficient Simulation of Post-Infarct Remodeling

MSc Research Thesis

Alessandro Tuttolomondo (5855160)*✉

*dept. BioMechanical Engineering, Faculty of Mechanical, Maritime and Materials Engineering, Delft University of Technology

Abstract - Post-myocardial infarction (MI) growth and remodeling (G&R), commonly referred to as fibrosis, involves both geometric deformation and progressive stiffening of infarcted tissue due to collagen accumulation. While zero-dimensional (0D) cardiac G&R models have successfully reproduced organ-level adaptations post-infarction, they often neglect evolving tissue properties associated with collagen turnover. In this study, we address this limitation by incorporating a time-dependent stiffening law into a strain-driven 0D framework, extending the original model by Witzenburg et al. (2018). Collagen turnover (CT) was modeled using a phenomenological exponential function, calibrated against experimental hydroxyproline data. The model was validated against independent canine datasets and benchmarked against both the original reference and a baseline No CT simulation. While full time-course verification was not achieved - due to inconsistencies in baseline reported parameters - control and acute states were accurately reproduced. Critically, the CT-enhanced model reduced the mean standardized z-score (MSZ) by 57.8%, with the most substantial improvements seen in ventricular volume and diastolic pressure predictions. These results confirm the added value of explicitly modeling tissue-level remodeling and highlight the importance of accurate initialization to ensure long-term prediction fidelity in reduced-order frameworks.

Cardiac Growth & Remodeling | 0D modeling | Collagen Turnover | Computational Cardiology

Advisor(s): dr. ir. Mathias Peirlinck, Ludovica Maga

1. Introduction

1.1. Relevance. Cardiovascular diseases (CVDs) represent a prominent global health concern which, according to recent studies, accounts for 37.5% of premature deaths from non-communicable diseases just in 2019 (1). Myocardial infarction (MI), with a global prevalence of 3.8% among individuals younger than 60 years and up to 9.5% in those older than 60 years, remains a major contributor to heart failure (HF), primarily due to irreversible damage to myocardial tissue and the subsequent maladaptive response that compromises left ventricular (LV) function (2, 3). Following an MI event, the heart undergoes a highly dynamic and time-dependent process of structural and mechanical adaptation known as growth and remodeling (G&R), where structural changes in

the myocardial extracellular matrix (ECM) impairs physiologic cardiac function and may lead to life-threatening complications such as infarct expansion, aneurysm, and HF (3). The healing process following MI can be divided into three overlapping and time-dependent phases – Figure 1. The acute phase (0–7 days) is marked by myocyte necrosis and inflammatory cell infiltration, accompanied by degradation of ECM proteins such as collagen and fibronectin, determining the infarct wall thinning (4). This is followed by the subacute phase (1–6 weeks), characterized by intense fibroblast activation and synthesis of new ECM components, particularly type I and III collagen, forming a provisional fibrotic matrix that stiffens the infarcted region (3). Finally, the chronic phase (>6 weeks) involves continued ECM remodeling and crosslinking, which further affects the mechanical integrity of the scar and the ventricular geometry (3). These dynamic changes are further amplified by neurohormonal feedback mechanisms and mechanical stimuli, which not only affect the infarct zone but also initiate eccentric hypertrophic remodeling in remote regions of the myocardium (4). This is a maladaptive compensatory mechanism which concerns an in-series deposition of sarcomeres that counteracts the loss of optimal contractile length of the LV, resulting into an increased ventricular mass while myocardial thickness experiences minimal changes (5, 6). Among the key drivers of the remodeling cascade, collagen turnover plays a central role in reshaping the mechanical behaviour of both infarcted and remote myocardial regions. Collagen turnover refers to the tightly regulated biochemical process by which collagen is synthesized, deposited, crosslinked, and degraded, ensuring the structural integrity and compliance of the cardiac ECM (7). In the context of MI, this homeostatic balance is severely disrupted, leading to the formation of a stiff, non-contractile scar in the necrotic zone. Macrophages represent the main drivers of collagen turnover by acting as early signaling hubs within the infarct zone (8). Through the secretion of cytokines such as TGF- β 1, they regulate both the recruitment and activation of cardiac fibroblasts, which differentiate into myofibroblasts - the principal source of collagen types I and III during the reparative phase (8). At the same time, macrophages modulate the expression of matrix metalloproteinases (MMPs), particularly MMP-2 and MMP-9,

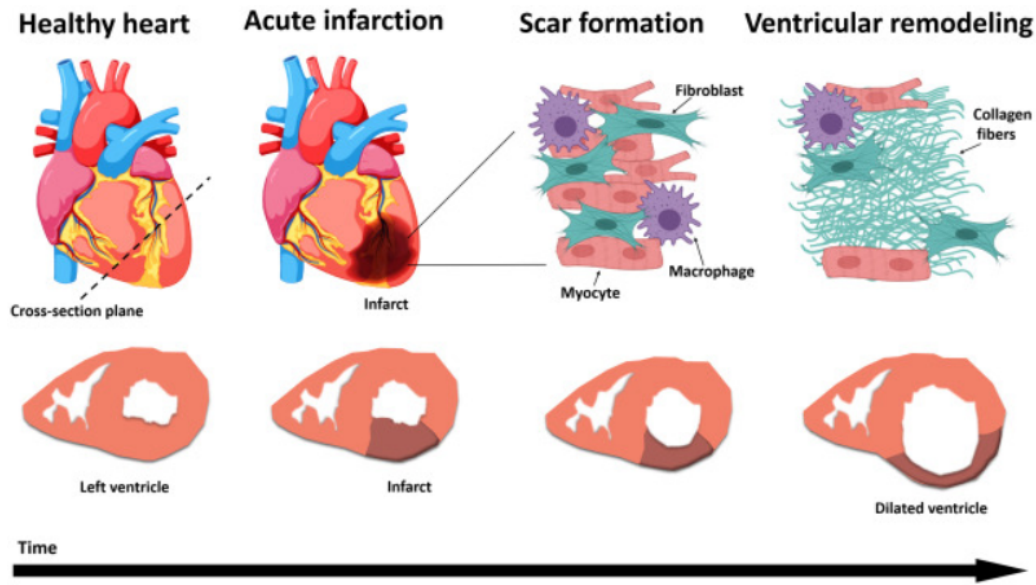


Fig. 1. Overview of the main biological mechanisms triggered during the post-MI healing process. Retrieved via: (4)

which mediate ECM degradation (8). This catabolic activity is finely balanced by the upregulation of tissue inhibitors of metalloproteinases (TIMPs), creating a feedback-controlled environment that determines scar composition and mechanics (8, 9). A visual breakdown of how the different biochemical actors contribute to collagen turnover is displayed in Figure 2. Importantly, experimental studies have shown that this remodeling is spatially heterogeneous: collagen accumulates not only in the infarct center and border zones but often also in non-infarcted regions such as the interventricular septum and right ventricular free wall, indicative of reactive interstitial fibrosis (7). From a biomechanical standpoint, collagen turnover progressively transforms the infarcted myocardium into an anisotropic, stiffened region, altering ventricular compliance and reshaping pressure-volume dynamics (3).

1.2. Motivation & Research Goal. Computational modeling has become an essential tool for multiscale investigation of (patho)physiological mechanisms that govern myocardial G&R (10–12). These models bridge microstructural processes - such as collagen turnover, myocyte hypertrophy, and ECM reorganization - with emergent changes in myocardial stiffness, chamber geometry, and global hemodynamics. As such, they represent a powerful tool for mechanistic insight,

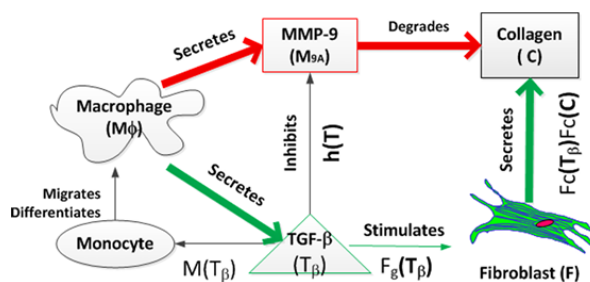


Fig. 2. Biochemical pathway and key factors that regulate collagen turnover mechanisms in the infarcted myocardium Retrieved via: (8)

in-silico hypothesis testing, and evaluation of patient-specific interventions (13). Among these, zero-dimensional (0D) - or lumped parameter (LPMs) - models provide a computationally efficient framework that captures cardiovascular dynamics at the organ scale. By solving time-dependent ordinary differential equations for pressure and flow across idealized compartments, 0D models can reproduce key features of cardiac performance and hemodynamic adaptation over extended simulation times with minimal computational cost (13, 14). This simplicity allows rapid testing of remodeling hypotheses and parameter sensitivity across long timescales, which is essential when simulating post-infarction progression or treatment effects. While high-fidelity 3D finite element (FE) models offer detailed spatial resolution, they are often impractical for iterative simulations or long-term remodeling studies. In contrast, 0D models excel in scenarios requiring repeated simulations, system-level coupling, or rapid parameter tuning. Their tractability also facilitates the integration of emerging biochemical mechanisms such as strain-driven growth stimuli (15–17). However, the majority of existent 0D frameworks for G&R rely on mechanically-driven volumetric growth formulations, which model geometric adaptation – such as wall thickening and cavity dilation – based on mechanical stimuli (15, 16). In volumetric growth models, it is often assumed that tissue properties remain constant and that processes linked to collagen remodeling are neglected. While this simplification facilitates tracking of geometric changes, it may limit the ability of such models to capture progressive diastolic stiffening, altered pressure-volume (PV) relationships, and maladaptive stress redistribution that characterize adverse post-infarction remodeling. We propose a computational model of myocardial post-infarction that couples strain-driven growth with a remodeling growth law based on collagen deposition. The presented approach builds upon an established 0D rapid compartmental model (16) and introduces a remodeling law

that evolves infarct material properties as a function of time, guided by hydroxyproline-based experimental data from canine subjects – a well-established surrogate marker for collagen content (7, 18). The primary objective of this work is to investigate how infarct stiffening influences PV behavior and whether incorporating tissue-level remodeling improves the predictive accuracy of low-dimensional cardiac simulations.

2. Methodology

The starting volumetric 0D model adopted in this study is taken from Witzenburg et al. (2018) (16) - see Figure 3 -, which successfully predicted the time course of three different hypertrophic conditions: pressure overload (PO), volume overload (VO), and MI.

The model combines a time-varying elastance (TVE) formulation for ventricular contraction with a lumped-parameter circulation and a strain-driven growth law that governs myocardial adaptation over time. Post-infarction adaptation was simulated by dividing the LV into two concentric compartments: a non-infarcted, contractile region and an infarcted, non-contractile region. The left ventricle was modeled as a thin-walled spherical chamber, with cavity volume and wall thickness evolving dynamically driven by the strain-based growth law fitted to experimental data. Unless otherwise specified, all baseline cardiovascular parameters were initialized to the optimized values reported by Witzenburg et al. (2018) (16) - see Appendix A.2. A remodeling law has been introduced to capture the progressive stiffening of the infarct during scar formation. Specifically, the diastolic stiffness parameter of the infarcted compartment was allowed to vary as a function of time, based on experimental hydroxyproline concentration and deposition dynamics from both canine and rodent studies (7, 18). This material property evolution was applied independently of the geometric growth update, which remained governed by deviations from the homeostatic myocardial fiber strain. The full model was implemented in Python 3.10 using a modular solver architecture. Growth was simulated over 42 days post-MI in discrete daily steps. The accuracy of the reproduced framework was verified against the original Witzenburg model, while the performance of the extended collagen turnover (CT)-enhanced model was validated against independent experimental data.

2.1. Circulation Model. The hemodynamic component of the model is structured as a closed-loop, lumped-parameter circulatory system comprising both systemic and pulmonary circulation, while explicitly modeling only the ventricular chambers. Each ventricle is modeled using a TVE formulation, and vascular networks are represented through Windkessel-like elements composed of resistances and compliances. Systemic and pulmonary circulations are implemented compliance–resistance–compliance (CRC) compartments, capturing pressure–flow relationships across the aortic, systemic, pulmonary, and venous beds. Cardiac valves are modeled as ideal diodes with forward flow resistances, opening and closing instantaneously based on pressure gradients. The TVE waveform is defined using a normalized cos-

inusoidal function, adapted from the original compartmental formulation by Santamore and Burkhoff (1991) (19). According to this formulation, the total ventricular pressure is computed as the sum of active and passive contributions:

$$P_{LV}(t) = P_{RV}(t) = e(t) [P_{ES}(V(t)) - P_{ED}(V(t))] + P_{ED}(V(t)) \quad (1)$$

where $V(t)$ is the instantaneous cavity volume, $e(t)$ is the TVE waveform, and P_{ES} and P_{ED} are the end-systolic and end-diastolic cavity pressures, respectively. Baseline End-systolic (ESPVR) and end-diastolic PV relationships (EDPVR) are computed for both ventricles following the methodology described by Witzenburg et al.;

$$P_{ES} = E \cdot (V_{ES} - V_0) \quad (2)$$

$$P_{ED} = B \cdot (\exp[A \cdot (V_{ED} - V_0)] - 1) \quad (3)$$

In these equations, P_{ES} and P_{ED} denote end-systolic and end-diastolic pressures, respectively. V_{ES} and V_{ED} are the corresponding chamber volumes, and V_0 is the unloaded volume. The parameter E represents the end-systolic elastance and defines the slope of the ESPVR, while A and B control the curvature and amplitude of the EDPVR, respectively.

From the onset of infarction – day 0 of growth – onward, the LV is further partitioned into two concentric compartments: a contractile, non-infarcted remote region and a non-contractile infarct zone. This structure follows the partitioning approach introduced by Sunagawa et al. (1983) (20), which assumes pressure continuity between compartments while allowing regional differences in passive properties and contractility. The total cavity volume is the sum of the sub-volumes of the remote and infarcted regions, with ventricular pressure calculated under the constraint of equal pressure across both regions.

To mathematically match this assumption, ESPVR and EDPVR of the LV have been restructured as follows for the healthy:

$$P_{ES} = E_h [V(t) - V_{0,h}] \quad (4)$$

$$P_{ED} = B_h (\exp[A_h (V(t) - V_{0,h})] - 1) \quad (5)$$

and the infarcted compartment:

$$P_{ES} = P_{ED} = B_i (\exp[A_i (V(t) - V_{0,i})] - 1) \quad (6)$$

where indices h , i refers to the healthy and infarcted compartments, and $V_{0,h}$ refers to unloaded cavity volumes. ES and ED parameters in eq. 2, 3 have been scaled according to the percentual extension of the infarcted – IS (%) – and non-infarcted compartment to maintain compartmental consistency of ESPVR and EDPVR - see Appendix A.3.1. The full system is solved using a set of ODEs governing pressure, volume, flow balance. At each time step, the flow across valves and vascular segments is computed using Ohm's law analogs: $Q = \Delta P / R$. Cardiac cycles are simulated over 2 seconds with 2000 time points, iterated until steady state is

Growth is applied exclusively in the non-infarcted myocardium, while the infarct zone is considered passive and non-contractile. However, mechanical coupling ensures that the infarct still influences growth in the remote region through shared pressure and geometry. At each step, the ESPVR and EDPVR parameters (A , B , E , V_0) of the non-infarcted myocardium are updated to reflect geometric adaptation:

$$V_0^i = \left(\frac{4\pi}{3}\right) \cdot (r_0 \cdot F_{g,f}^i)^3 \quad (14)$$

$$A^i = a \cdot \left(\frac{3}{4\pi}\right) \cdot \left(\frac{1}{r_0 \cdot F_{g,f}^i}\right)^3 \quad (15)$$

$$B^i = 2 \cdot b \cdot \frac{h_0 \cdot F_{g,r}^i}{r_0 \cdot F_{g,f}^i} \quad (16)$$

$$E^i = \frac{3}{2\pi} \cdot e \cdot \frac{h_0 \cdot F_{g,r}^i}{(r_0 \cdot F_{g,f}^i)^4} \quad (17)$$

r_0 and h_0 denote the baseline, before growth, unloaded radius and wall thickness, respectively. The directional growth components $F_{g,f}^i$ and $F_{g,r}^i$ represent the accumulated stretch in the fiber and radial directions at growth step i . The products between the original unloaded geometry and the accumulated growth stretch - $r_0 \cdot F_{g,f}^i$ and $h_0 \cdot F_{g,r}^i$ - represent the new unloaded radius r_0^i and thickness h_0^i computed at each growth step. Passive and active material properties in the non-infarcted tissue (a , b , and e) remain constant at their pre-growth values throughout the simulation. In contrast, infarct stiffness (parameter b) is allowed to vary over time to reflect collagen turnover - see Section 2.3. Systemic parameters such as heart rate (HR) and systemic vascular resistance ($R_{a,s}$) are time-dependent and updated based on experimental post-MI data from Jugdutt et al. (1995) (18). Additionally, an evolving infarct size (IS%) is implemented over time, following trends reported in the same dataset. An overview of the simulation pipeline is provided in Figure 4.

2.3. Tuning Baseline and Acute Hemodynamics. To initialize the growth and remodeling simulation, hemodynamic conditions at baseline (day -1) and acute post-infarction (day 0) were first established. This was achieved by implementing the set of control and acute circulatory parameters reported by Witzenburg et al. (2018) (16) tuned to the myocardial infarction study by Jugdutt et al. (1995) (18). These include systemic resistance, stressed blood volume (SBV), heart rate, and ventricular ESPVR and EDPVR parameters. All values are available Appendix A.2. These values were used as input to simulate the hemodynamic state at day -1 (control) and day 0 (acute), prior to any remodeling. The implemented hemodynamic framework was initialized with the baseline ESPVR and EDPVR (eq: 2, 3) for the control simulation. From the acute simulation onward, where myocardial infarction was introduced, the ESPVR and EDPVR

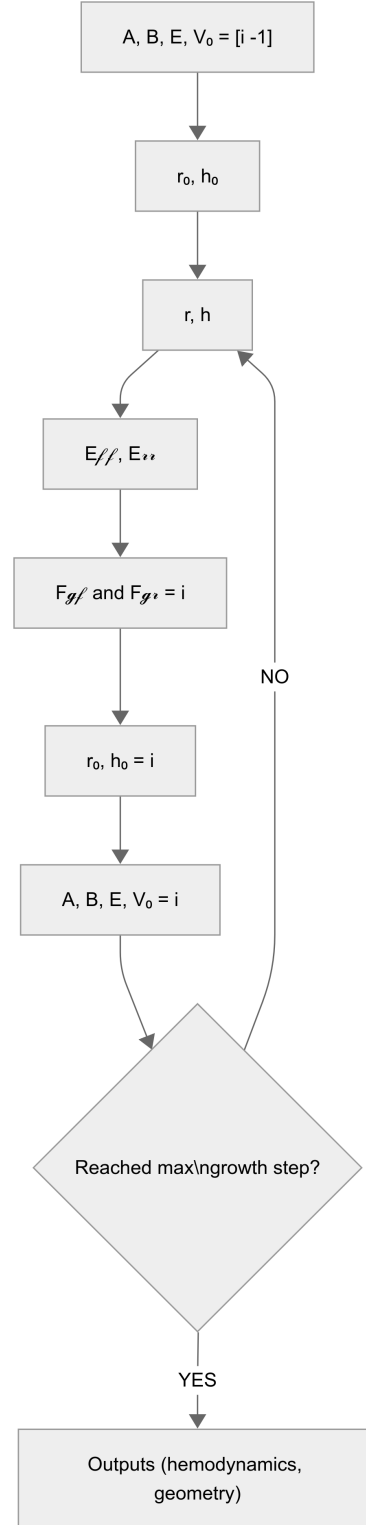


Fig. 4. Schematic overview of the Growth Framework algorithm. Unloaded (r_0 and h_0) and loaded (r and h) geometries are computed from the previous step's hemodynamic parameters and outputs. Fiber and radial strains are used to compute the growth stimulus, which updates the deformation gradient. Resulting growth stretches are then multiplied by the baseline unloaded geometry to obtain the current unloaded radius and thickness. These are used to retrieve new geometrical and hemodynamic parameters (Eq. 14 - 17) as new inputs to the circulation model. The loop is repeated until the 42-day endpoint is reached.

relations used were those described in equations 4 - 6 which explicitly model the left ventricle as a composite of infarcted and non-infarcted compartments. To ensure physiological consistency between the two ventricular regions, two root-finding optimizations were performed at each iteration using Python's `fsolve` function. These solvers enforce pressure continuity at both end-diastole and end-systole by adjusting sub-compartment volumes so that the computed P_{ED} and P_{ES} match across the infarcted and remote regions. The simulation outputs were then compared with those reported by Witzenburg - see Section 3.1. Additionally, prior to the initialization of the growth simulation, the left ventricular wall volume (V_{wall}) was iteratively optimized to match the end-diastolic thickness ratio ($h_{ED}/h_{ED,0}$) reported by Witzenburg for the remote myocardium at baseline. This was done by adjusting V_{wall} until the loaded geometry, computed through the thin-walled spherical assumption, reproduced the correct myocardial thickness at end-diastole. The corresponding unloaded and loaded geometry equations used for this optimization—based on cavity volume V_0 and wall volume V_{wall} —are provided in Appendix A.3.2.

2.4. Collagen Turnover Modeling. To simulate the biomechanical effects of post-infarction scar formation, a time-dependent remodeling law was introduced to represent progressive stiffening of the infarcted myocardium. While growth was limited to the healthy LV compartment and simulated as described in Section 2.2, the effects of collagen turnover-driven stiffening were incorporated in the infarcted region. The material parameter b of the infarcted compartment, which represents its passive stiffness, was allowed to evolve over time. The choice of b was motivated by its direct relationship with the parameter B in the exponential EDPVR formulation, expressed at baseline as:

$$b = \frac{B \cdot r_0}{2 \cdot h_0} \quad (18)$$

While both coefficients A and B shape the diastolic pressure-volume curve (eq. 3), B acts as a linear amplitude scaler and has a dominant influence on early diastolic stiffness. In contrast, A controls the exponential curvature and is more sensitive to unphysiological dilation. Therefore, updating b in the infarcted compartment enables a direct and numerically stable control of the infarct stiffening over time while preserving the EDPVR structure used throughout the model. Due to the rapid collagen deposition that characterized the first 6 weeks of post-MI remodeling, we modeled collagen deposition over time by an exponential function that describes the temporal dynamic of passive stiffness variable:

$$b(t) = b_0 + (b_{max} - b_0) \cdot [1 - \exp(-kt)] \quad (19)$$

where b_0 is the passive stiffness prior to any growth, $b_{max} = b_{mult} * b_0$ is the asymptotic infarct stiffness, k is the collagen deposition rate controlling the stiffening speed, and t (days) is the G&R simulation time. Experimental data from Jugdutt et al. (1995) (18) was used to define a plausible tuning range for the b_{mult} stiffening parameter, based on hydroxyproline concentrations measured in canine myocardium at

six weeks post-MI. Concurrently, rodent studies (7, 8) have shown that collagen accumulation generally reaches a plateau within the first 10–14 days, which informed the tuning range for the growth rate constant k . The parameters b_{mult} and k were identified by minimizing an objective function which quantifies the error between simulation outputs and experimentally reported targets (18):

$$\mathcal{J}(k, b_{mult}) = \frac{1}{N} \sum_{j=1}^N \left(\frac{y_j^{model}(k, b_{mult}) - \mu_j^{exp}}{\sigma_j^{exp}} \right)^2 \quad (20)$$

These targets included end-diastolic pressure (EDP), mean arterial pressure (MAP), minimum and maximum left ventricular (LV) volume, and normalized LV wall thickness. Based on this function, mean squared z-scores (MSZ) for each target over the relative time points have been computed - see details in Appendix A.4. Finally, the reduction of the total average MSZ was set as the optimization goal. Parameter identification followed a two-step procedure. First, a coarse parameter grid was constructed to explore physiologically plausible combinations. The resulting z-score-based error surface is shown in Figure 5 and was used to identify candidate regions of minimal discrepancy between model predictions and experimental data. Subsequently, the three best-performing candidates from the grid were selected as initial guesses for a constrained optimization with the Powell algorithm (23). This derivative-free method iteratively refines the parameter values by performing sequential line minimizations along a set of directions, making it suitable for smooth but potentially non-differentiable objective functions. This strategy allowed for robust calibration of infarct material properties that reflect both the experimental time course of collagen accumulation and the hemodynamic effects of infarct stiffening. The resulting time-varying $b(t)$ was applied exclusively to the infarcted compartment and updated at each growth step.

2.5. Verification and Validation. To assess the accuracy and reliability of the proposed growth and remodeling framework, both verification and validation procedures were performed. Verification was conducted using the implemented model without the CT remodeling law, ensuring consistency with the original formulation by Witzenburg et al. (2018) (16). A first verification step was the quantification of target hemodynamic outputs for the control and acute simulations. Simulations were run under identical conditions and parameter settings, and model predictions were compared against experimental data to confirm that the framework reproduced the original model's fitting performance. A verification was deemed successful when the relative difference between key model outputs—namely mean arterial pressure (MAP), mean left atrial pressure (MLAP), end-systolic and end-diastolic LV volume, and normalized ED wall thickness—remained within 15% of the reference values reported by Witzenburg. To verify model performance over 6 weeks of G&R, the resulting trajectories of the key hemodynamic

Table 1. Verification of control and acute hemodynamic simulations. Model outputs are compared to Witzenburg et al. (2018). Relative error is calculated as: $(\text{Model} - \text{Witzenburg}) / \text{Witzenburg} \times 100$. All results fall within the $\pm 15\%$ verification threshold.

Metric	Witzenburg	Model	Error (%)
Control (Day -1)			
ED Volume (ml)	47.8	47.7	-0.21%
ES Volume (ml)	25.5	25.7	+0.78%
Mean Aortic Pressure (mmHg)	114.3	114.4	+0.09%
Mean Left Atrial Pressure (mmHg)	5.6	6.3	+12.50%
ED Thickness Ratio ($h_{ED}/h_{ED,0}$)	-	-	-
Acute (Day 0)			
ED Volume (ml)	72.2	72.5	+0.42%
ES Volume (ml)	46.3	46.7	+0.86%
Mean Aortic Pressure (mmHg)	112.3	112.4	+0.09%
Mean Left Atrial Pressure (mmHg)	18.3	18.7	+2.19%
ED Thickness Ratio ($h_{ED}/h_{ED,0}$)	0.96	0.96*	0.00%

* Value was explicitly optimized to match the target value reported by Witzenburg et al. at day 0.

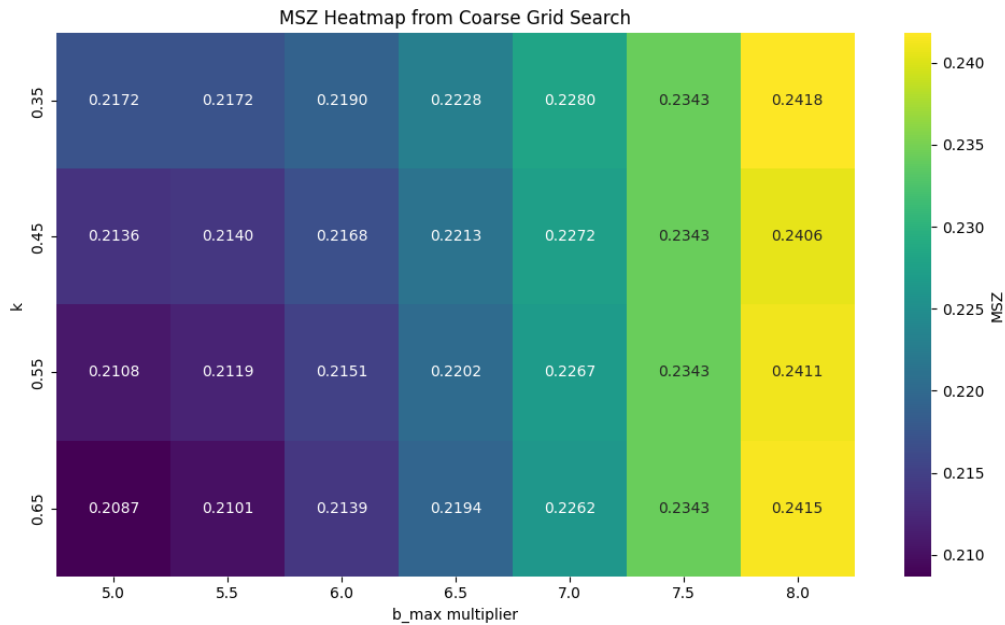


Fig. 5. Z-score-based error surface used to identify optimal collagen turnover parameters. The heatmap displays the total mean standardized z-score (MSZ) across five key hemodynamic variables as a function of the infarct stiffening rate constant k and stiffness multiplier b_{mult} . Regions with lower MSZ values correspond to better agreement with experimental data and were used to initialize the local optimization step.

targets were compared with the results obtained by Witzenburg et al. A close match at any time of the simulation time course indicates a successful verification. Validation of the extended model - including the time-dependent infarct stiffening formulation - was performed using independent experimental data from Jugdutt et al. (1995) (18). In both verification and validation, model outputs were evaluated against five key hemodynamic variables: maximum and minimum LV volume, EDP, MAP, and normalized ED wall thickness. Model performance was quantified using z-scores and the mean squared z-score (MSZ). A z-score indicates whether the model over- or underestimates a quantity, and by how much,

relative to the variability observed in experimental data. A z-score that falls below 1.0 indicates that the value is within the standard deviation (SD) of experimental data, while a lower score indicates better agreement with the mean SD. To assess overall accuracy, MSZ values were computed for each output variable and averaged to yield a single score. The results of these procedures are presented in the following section.

3. Results

3.1. Model Verification. The proposed G&R framework was evaluated against the original results reported by Witzenburg et al. (2018) (16). Simulations were conducted without

Table 2. Mean standardized z-scores (MSZ) for each key variable across the Witzenburg reference, No CT baseline, and CT-enhanced models. Lower MSZ values indicate better agreement with experimental data. Validation is considered successful for $MSZ < 1$ across all variables.

Parameter	Witzenburg Model	No CT Model	CT Model
Max LV Volume	0.17648	0.18306	0.08928
Min LV Volume	0.82835	0.66181	0.04626
End-Diastolic Pressure (EDP)	0.10640	0.56794	0.20341
Mean Arterial Pressure (MAP)	0.10063	0.27841	0.27332
Normalized ED Wall Thickness	0.26318	0.78104	0.43108
Average MSZ	0.29501	0.49445	0.20867

incorporating collagen turnover, and key simulation outputs were compared both qualitatively and quantitatively to verify that the baseline model behavior aligned with the original reference framework. Table 1 shows a comparison between this model’s outputs and those reported by Witzenburg prior to growth. Each of the reported variables shows strong agreement with Witzenburg’s results (error $< \pm 1\%$). One exception is presented in MLAP, particularly in the control simulation. However, the reported values for this variable are well within the set verification threshold. The quantitative agreement achieved at this stage confirms that the reimplementation correctly reproduces the baseline and acute hemodynamics of the original framework. Figure 6 (a-e) shows the long-term evolution of the key hemodynamic and geometric variables, which are plotted alongside the Witzenburg data and experimental measurements. Overall, the time-course results of the baseline model without collagen turnover show key remodeling trends; yet, we note discrepancies in early estimation for all the target variables. In summary, the reimplementation successfully reproduces the control and acute conditions but does not fully replicate Witzenburg’s reported post-MI evolution across all variables. As a result, time-course verification of the growth behavior falls outside the defined $\pm 15\%$ error margin. Since the early discrepancies have been thoroughly investigated (see Section 2.3), the baseline No CT simulation will be adopted as the internal reference for evaluating the performance of the collagen turnover-enriched implementation presented in the following sections.

3.2. CT Function Optimization. The parameters governing infarct stiffening, b_{mult} and k , were optimized to minimize the total MSZ across the five key output variables. As previously described, during the first phase of the optimization, a coarse parameter grid – whose bounds were estimated based on experimental observations of collagen deposition rate and concentration – was explored to identify regions of low MSZ. The corresponding z-score-based error surface is displayed in Figure 5. The three best-performing parameters – in the range $k = [0.55, 0.65]$ and $b_{\text{mult}} = [5, 5.5]$ – were used to initialize a constrained Powell optimization for local refinement. The final optimized values were $b_{\text{mult}} = 5.08$ and $k = 0.6468$. These parameters produced the lowest overall MSZ and were used in the subsequent validation simulation.

3.3. Model Validation. The predictive capability of the proposed framework was assessed by comparing both the baseline (No CT) and collagen turnover-enhanced (CT) simulations against experimental data from Jugdutt et al. (1995) (18), which was also used for validation in the original Witzenburg et al. study. This comparison evaluates whether the incorporation of a time-varying infarct stiffening law improves agreement with post-MI remodeling trends. As discussed in Section 4.1, while the verification of long-term G&R time courses was not achieved - due to diverging trajectories relative to the original model, the present validation focuses on the model’s ability to reproduce experimental outcomes. Overall, Figure 6 shows that both No CT and CT simulations capture key qualitative features of post-infarction remodeling, including the decline in EDP, partial recovery of MAP, and progressive chamber dilation and wall thickening. However, the inclusion of collagen turnover (CT model) significantly reduces the model-experiment error for nearly all variables. Quantitative performance is summarized in Table 2, which reports the mean standardized z-scores for each output. Compared to the No CT simulation, the CT model shows substantial error reduction in all variables except MAP, where performance remains similar. The largest improvements are seen in minimum and maximum LV volumes, with MSZ reductions of 93.0% and 51.2%, respectively. EDP and normalized wall thickness also show substantial improvements (64.2% and 44.8%), while MAP shows comparable performance between the two models. Overall, the average MSZ decreases from 0.494 (No CT) to 0.209 (CT), corresponding to a 57.8% improvement. These results confirm that incorporating collagen turnover significantly enhances the model’s ability to reproduce experimental post-MI remodeling behavior, validating the effectiveness of the proposed stiffening law.

4. Discussion

The presented results demonstrate that the proposed 0D growth and remodeling framework successfully captures essential features of post-MI ventricular adaptation and that the inclusion of a collagen turnover-driven remodeling law significantly improves the model’s ability to reproduce experimental trends. While the baseline implementation does not fully verify the time course of Witzenburg’s growth trajectories, the enhanced model achieves a strong validation against

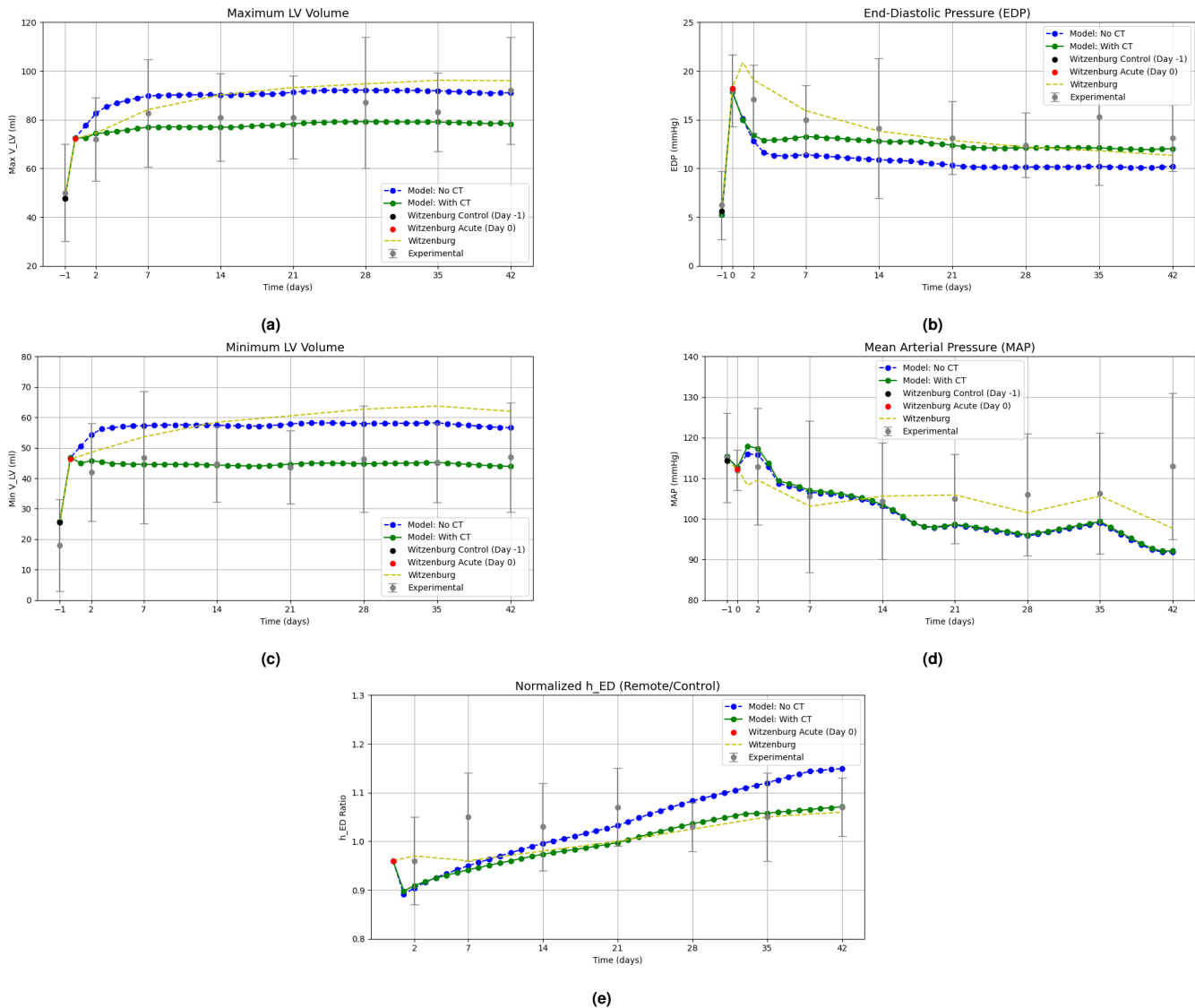


Fig. 6. Time course of key physiological variables during post-MI remodeling: (a) maximum LV volume, (b) EDP, (c) minimum LV volume, (d) MAP, and (e) normalized ED wall thickness. The blue curve *-No CT-* refers to the baseline simulation used for verification. The green *-CT-* curve refers to the simulation where the model embeds the collagen turnover exponential remodeling law, used for validation. The yellow curve refers to the outputs from Witzenburg et al. (2018) (16). The gray experimental points with their SD are reported from the chosen dataset (18).

independent experimental data. Both qualitative evolution and quantitative metrics support the benefit of incorporating infarct stiffening into low-dimensional cardiac models.

4.1. Prediction Accuracy. When comparing the No CT baseline simulation to the original Witzenburg model, the qualitative evolution of key parameters appears broadly consistent, particularly in trends like progressive cavity dilation, remote wall thickening, and EDP reduction over time. However, a clear discrepancy emerges at day 1 of growth, where a discontinuity is observed in nearly all key variables. For instance, EDP (Figure 6b) in the No CT model rapidly declines after the acute phase, in contrast to the sustained elevation observed in the original reference. Similarly, the ED thickness ratio (Figure 6e) shows an early dip followed by monotonic thickening, whereas Witzenburg’s curve remains relatively flat during this period. A moderate misalignment is shown for MAP (Figure 6d) and both LV volumes (Figures 6a and

6c) during this window. This early divergence persists during the acute-to-subacute transition and affects the model’s ability to reproduce Witzenburg’s remodeling trajectory. A plausible explanation for this mismatch lies in the input data adopted from Witzenburg et al. (Appendix A.2), both for the pre-growth hemodynamic conditions and the growth initialization - see Section 2.3. These values were used to compute the LV wall volume and establish the baseline unloaded geometry. However, this setup likely results in an inaccurate calculation of the fiber and radial growth stretches (eq. 12 and 13) at the first growth step, due to a misalignment between baseline strain setpoints and acute loading conditions. The resulting discontinuity initiates an error cascade that limits the model’s fidelity in early remodeling. Due to this mismatch, the No CT simulation does not replicate Witzenburg’s G&R trajectories across the full 6-week timeline, and time-course verification cannot be claimed. Nevertheless, the successful verification of the control and acute

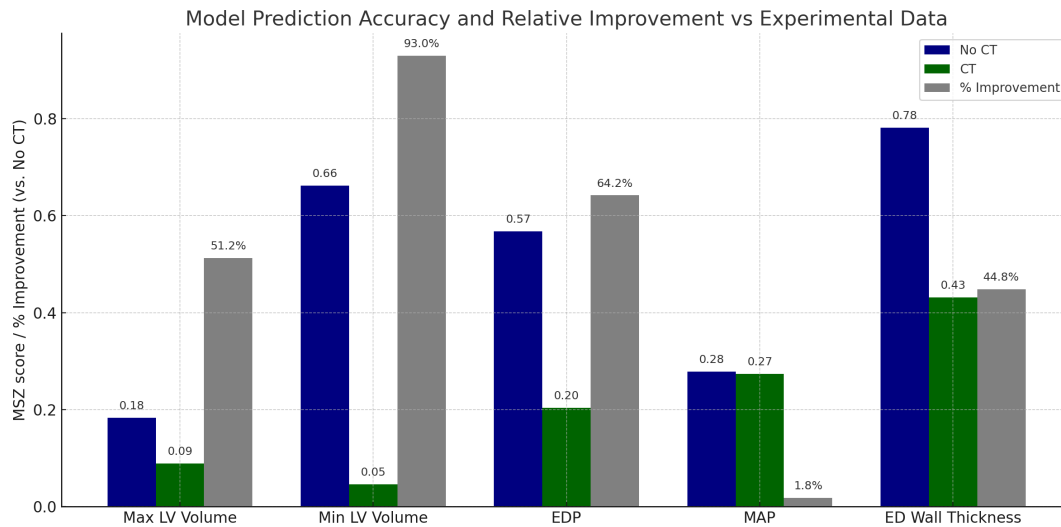


Fig. 7. Model prediction accuracy and relative improvement across key output variables. Bars show mean standardized z-scores (MSZ) for the No CT (blue) and CT (green) models. Gray bars indicate the relative improvement in prediction accuracy achieved by incorporating collagen turnover, computed as the percentage reduction in MSZ from the No CT model.

hemodynamic states (Section 3.1) confirms that the model reproduces the correct physiological regime at initialization. Given that the growth law and solver architecture were carefully reconstructed based on Witzenburg’s description, we deemed this level of consistency sufficient to proceed with collagen turnover modeling. This decision is further justified by the clear gains observed after integrating collagen turnover. The optimized CT-enhanced model consistently reduces z-score errors across all tracked variables (except MAP, which remains stable), leading to a 57.8% improvement in overall MSZ. An overview of the percentual improvements over the target hemodynamic and geometric outputs is shown in Figure 7. These outcomes support the model’s credibility and highlight the practical value of incorporating microstructural remodeling into rapid simulation tools.

4.2. Modeling CT. The significance of infarct stiffening during post-MI remodeling has been underscored in various experimental and computational studies. The framework developed in this work extends the volumetric G&R model proposed by Witzenburg et al. (2018) (16) by explicitly incorporating the effects of collagen turnover through a time-dependent passive stiffness law. This extension allows for a more physiologically grounded representation of infarct maturation, aligning with biochemical and histological observations of collagen accumulation in the healing myocardium. In the original Witzenburg formulation, infarct properties were assumed to remain fixed throughout the simulation, and scar tissue mechanics was indirectly handled through geometric remodeling of the healthy remote myocardium. While this simplification allowed for reproducing broad trends in post-MI adaptation, it neglected the progressive stiffening of scar tissue known to occur during healing. The addition of a CT-driven law addresses this limitation and aligns the model more closely with experimental findings from Jugdutt et al. (1995) (18) which demonstrated a substantial increase in hydroxyproline concentration – a surrogate for collagen con-

tent – over the first six weeks post-infarction in canine myocardium. Specifically, collagen content was found to be approximately 4-fold higher in the infarct border zone and up to 10-fold higher in the infarct center compared to the remote posterior wall, where no significant increase was detected. The final stiffness scaling factor - b_{mult} - obtained through model optimization falls well within this experimentally observed range, providing physiological support for the model’s material parameterization. As no collagen deposition rates were explicitly reported by Jugdutt et al. (1995) (18), further support for the time course of collagen accumulation is found in rodent studies, such as Cleutjens et al. (2019) (7), which described a rapid rise in collagen expression and deposition within the first two weeks post-MI, followed by stabilization. Although these studies are conducted in small animals and are not directly translatable to the canine model, the general trend – a steep early-phase rise in stiffness – aligns with the exponential formulation adopted here. The optimized rate constant - k - captures this accelerated stiffening phase, offering a parameterization consistent with both biochemical and histological timelines. Other experimental studies provide further quantitative backing. Uusimaa et al. (1997) (24) tracked collagen scar formation in patients using PIIINP levels as a proxy for collagen turnover and reported a significant rise during the first 3–4 days, with sustained elevated levels for at least 10 days post-MI. Rusu et al. (2019) (25) used murine models and found that type I collagen became dominant by day 14 post-MI, while type III peaked earlier and declined thereafter. The range selected for b_{mult} and k during optimization was thus informed by these findings. However, the heatmap of the z-score surface (Figure 4) shows a strong dominance of the rate constant k in driving the error reduction, suggesting that even lower MSZ values might be achieved for higher k values, potentially outside the selected physiological range. Nonetheless, the final parameter set achieves a physiologically realistic infarct stiffening curve, which is comparable to the reported 4–10 x increase

in infarct collagen content and with the temporal dynamics of collagen accumulation described across multiple species. This supports the validity of the exponential formulation and the constrained optimization strategy adopted in this work. Overall, the inclusion of infarct stiffening led to notable improvements in model performance, particularly for volume-related and EDP outputs. The CT-enhanced model improved prediction accuracy. These results confirm that integrating collagen turnover into reduced-order G&R frameworks not only enhances physiological relevance but also yields more accurate, data-driven simulations of post-infarct remodeling. In summary, the proposed approach incorporates collagen turnover into G&R frameworks and offers a pathway for linking histological markers of scar maturation with macroscopic functional outcomes.

4.3. Limitations. While the presented framework successfully reproduces key features of post-infarction remodeling and offers a physiologically motivated representation of infarct stiffening, some limitations should be acknowledged.

4.3.1. Early Discrepancies: Tuning Baseline Parameters. Although the baseline and acute hemodynamics were successfully verified (Section 3.1), early mismatches were observed during the first post-infarction growth step (day 1), where a sharp discontinuity is observed in multiple output variables, most notably in EDP and the normalized LV wall thickness ratio. In the original Witzenburg simulation, EDP displays an early post-MI peak that reflects the transient increase in preload due to infarct-induced pump dysfunction. This feature is consistent with physiological expectations and experimental observations. However, in the present model, this behavior is absent: EDP does not rise but instead begins a gradual decline immediately after the infarct event. At the same time, the wall thickness ratio undergoes a sudden drop, followed by an unphysiological overshoot in subsequent days. This anomalous behavior suggests that the growth stretches computed at day 1 - both in the fiber and radial directions - were inaccurately estimated. Since these quantities directly govern the update of the unloaded geometry and the subsequent derivation of EDPVR and ESPVR parameters, any error in their computation is rapidly propagated throughout the growth simulation. A likely root cause of this issue is the erratic optimization of the initial LV wall volume (V_{wall}), which was tuned to match the reported end-diastolic thickness ratio in the acute post-MI state. To investigate this hypothesis, an auxiliary optimization was performed in which V_{wall} was computed from Witzenburg's reported end-systolic and end-diastolic volumes for both control and acute conditions, while also being constrained to match the reported end-diastolic thickness ratio and the baseline fiber ($E_{\text{ff},0}$) and radial ($E_{\text{rr},0}$) strains. Importantly, the values of $E_{\text{ff},0}$ and $E_{\text{rr},0}$ used in this simulation were directly adopted from Witzenburg et al. (2018) (16). The results of this constrained optimization revealed that no single value of V_{wall} could simultaneously satisfy all three constraints. The derived geometry suggested a possible overestimation of $E_{\text{ff},0}$ and $E_{\text{rr},0}$. This mismatch leads to an artificially small growth stimulus in the

fiber direction (eq. 10), driving an exaggerated increase in the fiber growth stretch and an inflated unloaded cavity radius r_0 . At the same time, a higher value of $E_{\text{rr},0}$ could contribute to an overestimated unloaded wall thickness h_0 , which further distorts model dynamics. Since parameters A , B , and E depend nonlinearly on both r_0 and h_0 (eq. 15 - 17), this combination of geometric distortion severely affects the mechanical behavior computed in the first growth step. In particular, these updated parameters are then used by the circulation model's nonlinear solvers to enforce pressure continuity across the infarcted and remote compartments. Specifically, two `fsolve` operations are performed at each growth step to ensure that pressures at end-diastole and end-systole match between regions. When the underlying geometry—and thus the pressure-volume relationships—are distorted, these solvers are forced to identify non-physiological compartmental volumes to reconcile pressure mismatch. As a result, even small errors in initial geometry can propagate and amplify through the model, leading to visible deviations in pressure and wall thickness as early as day 1. To further investigate this initialization mismatch, the optimization procedure was extended to also explore the impact of the reported baseline unloaded volume (V_0), due to its dominant influence on the computed unloaded radius r_0 . A two-dimensional parameter sweep was performed to identify the combination of V_{wall} and V_0 that best satisfies all three constraints simultaneously: the reported end-diastolic LV wall thickness, and the fiber and radial strain setpoints $E_{\text{ff},0}$ and $E_{\text{rr},0}$. Details of this optimization strategy are provided in Appendix A.6. As shown in Figure 8, no single value of V_{wall} could satisfy all three constraints simultaneously, even when allowing V_0 to vary within a physiologically reasonable range. However, the degree of mismatch was reduced for higher values of V_0 , suggesting that the baseline unloaded volume reported in the original dataset may be slightly underestimated. This suggests that at least one of these reference values is likely inaccurate or incompatible with the others. While these early mismatches prevented complete time-course agreement with Witzenburg's results, they do not compromise the physiological validity of the framework. Rather, they highlight the need for joint reparameterization of geometric and hemodynamic baseline and acute input parameters before G&R initiation - including V_0 , V_{wall} , and the strain setpoints. The robustness of the collagen turnover model was instead evaluated using the internally consistent No CT simulation as the reference case.

4.3.2. Spatial Characterization. The OD framework adopted in this study does not resolve regional heterogeneity within the ventricular wall. While infarct and remote regions are represented as separate compartments, the model assumes uniform properties within each, thereby omitting spatial gradients in stiffness, strain, or collagen content, especially across the infarct border zone. These simplifications are intrinsic to the lumped-parameter formulation and limit the model's ability to capture localized remodeling behavior.

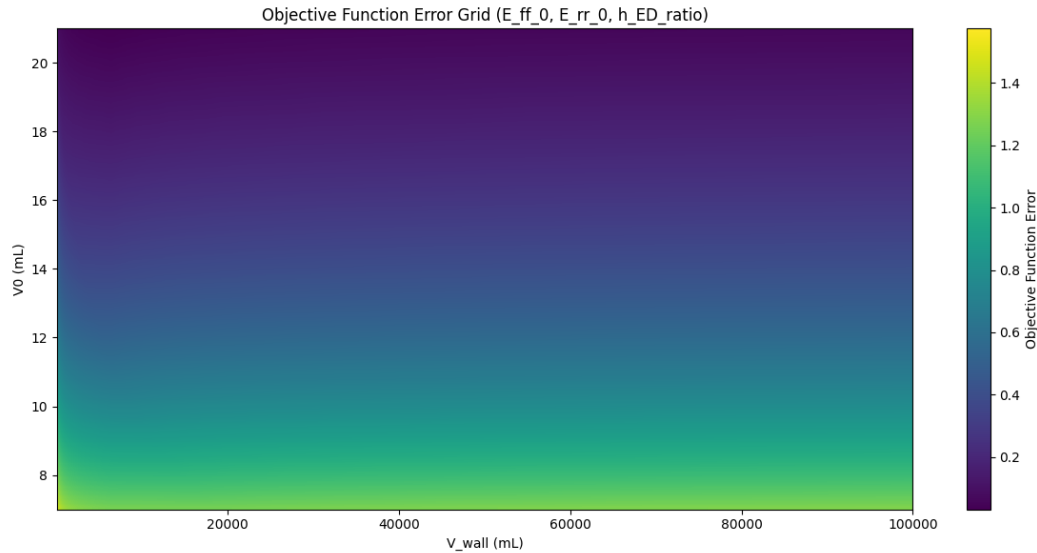


Fig. 8. Objective function error surface for combinations of unloaded volume (V_0) and wall volume (V_{wall}), constrained to simultaneously match the reported ED thickness ratio, fiber strain $E_{f,0}$, and radial strain $E_{r,0}$. Darker regions correspond to lower objective function error. No single pair of values perfectly satisfies all three constraints, although improved agreement is observed for higher values of V_0 , suggesting a possible underestimation in the reported baseline geometry.

4.3.3. Phenomenological Simplifications. Several simplifications were made in modeling collagen turnover to ensure tractability and consistency with experimental data. The CT mechanism is modeled purely phenomenologically through an exponential increase in passive stiffness, informed on experimental concentration trends. Although this approach provides an effective approximation of macroscopic stiffening, it does not directly account for the underlying cellular processes, such as fibroblast activation, MMP/TIMP regulation, or the interplay between different collagen subtypes. Additionally, no explicit feedback from mechanical loading to collagen deposition is modeled, which limits the framework's capacity to capture mechano-sensitive remodeling pathways. Another key assumption of this model was the use of a 1:1 correlation between collagen concentration and infarct stiffness when defining the initial parameter boundaries for optimization. While hydroxyproline content is a widely used proxy for collagen, infarct stiffness is also modulated by other ECM components such as elastin, fibronectin, and cross-linking enzymes. Furthermore, the CT law was applied only to the infarcted myocardium, while the material properties of the remote healthy region were kept constant. This decision was supported by the findings of Jugdutt et al. (1995) (18), which reported no significant change in hydroxyproline content in the noninfarcted posterior wall after six weeks of healing, but it is not universally applicable. Importantly, the collagen deposition rate of the current model's exponential stiffening law was parameterised based on rodent data, where infarct collagen typically plateaus within 14 days. In contrast, Jugdutt et al (1996) (26) reported a slower progression in canine models: 1.5-fold increase at week 1, 4-fold by week 2, 7-fold by week 3, and levelling off at 8-11x by day 50. This suggests a more sigmoidal collagen deposition pattern in large-animal models compared to the rapid exponential rise observed in rodents. To reflect this, an alternative sig-

moidal law (see Appendix A.5) has been developed. While it qualitatively captured the progressive stiffening profile and yielded comparable accuracy in predicting key parameters such as EDP and LV volumes, it required three parameters to optimize, increasing the computational cost significantly. Due to its comparable performance and greater complexity, it was not selected for the final model implementation.

5. Model Potentialities & Future Outlooks

A key strength of the framework developed by Witzenburg et al. (2018) - and extended in this study - is its modular structure, which enables reparameterization across species and experimental conditions. In this work, the original baseline and acute circulatory parameters fitted to a canine MI dataset by Jugdutt et al. (1995) were reused to preserve continuity with the reference model. However, the root-cause analysis of early remodeling discrepancies suggests that some of these baseline inputs—particularly those governing geometry and strain setpoints—may require joint refinement to ensure internal consistency when used as initial conditions for growth. This insight opens a clear direction for future improvement: refining the model's initialization pipeline using multi-constraint optimization, in which geometric, hemodynamic, and mechanical targets are jointly satisfied. Doing so would improve the alignment of fiber and radial strain with actual loading states and minimize artificial growth triggers at the onset of remodeling. Despite these initialization challenges, the independently optimized collagen turnover law demonstrated strong predictive power when validated against experimental data, significantly improving z-score accuracy across key variables. While the infarct stiffening multiplier (b_{mult}) was tuned using canine data, the time constant k was derived from rodent collagen kinetics due to limited time-resolved datasets in large animals. The framework thus remains adaptable: it can accommodate species- or region-

specific remodeling profiles, and be extended or recalibrated as new data emerge. As such, this work lays the foundation for broader applications of low-dimensional G&R modeling in both translational and experimental settings. Building on this foundation, future applications could explore reparameterization of both the G&R framework and the CT function using rodent models, where collagen is in minor concentration and often extends to non-infarcted regions as well. For example, Cleutjens et al. (1995) (7) observed collagen gene expression and ECM remodeling activity even in the remote non-infarcted myocardium of rats, suggesting that species-specific remodeling signatures may require distinct spatial and temporal parameter sets. Adapting the model to such conditions would represent a critical step toward cross-species generalizability, broadening its utility in both preclinical and translational research. Additionally, due to its modular design and previous application to other hypertrophic conditions by Witzenburg et al. (2018), the current framework could be extended to study fibrotic remodeling under pressure overload (PO). In canine PO models, Nagatomo et al. (1999) (27) demonstrated a significant increase in protein synthesis—particularly myosin heavy chain—via upregulated translational efficiency and capacity. These findings imply an active fibrotic and hypertrophic response to elevated wall stress, which the present CT framework holds potential to capture, if growth triggers and timescales are appropriately adjusted for pressure-overload conditions. Despite its reduced-order formulation, the current framework also holds potential to inform or be coupled with higher-dimensional finite element (FE) models. The infarct stiffness evolution derived from the CT law could be mapped onto region-specific strain energy density functions in 3D simulations. This approach aligns with the strategy proposed by Sáez et al. (2013) (9), who developed a constitutive formulation for collagen turnover responsive to local stress and biochemical stimuli. Embedding the present CT-driven stiffness formulation into FE frameworks could enable spatial characterization of remodeling, bridging microstructural mechanisms with organ-level mechanics. Finally, the current phenomenological CT law could be enriched by coupling with biochemical models that describe collagen synthesis and degradation pathways in a mechanistic manner. The mathematical model developed by Jin et al. (2011) (8) offers an example of such an approach, quantifying the interplay between TGF- β signaling, MMP/TIMP regulation, and fibroblast activity. Linking such a biochemical module to the current stiffness-based framework would allow dynamic prediction of collagen concentration based on upstream cellular signaling, further enhancing physiological interpretability and cross-modal validation.

6. Conclusion

This thesis presented a collagen turnover-enhanced OD growth and remodeling framework for simulating ventricular adaptation following myocardial infarction. By extending an established compartmental model with a physiologically motivated infarct stiffening law, the simulation captured both geometric and material remodeling with improved predictive

accuracy. Although the verification of long-term G&R trajectories failed due to initialization inconsistencies - likely stemming from conflicting baseline parameters - the framework reliably reproduced the control and acute post-MI states. Validation against experimental data confirmed the benefit of incorporating collagen turnover, particularly in improving the prediction of cavity volumes and end-diastolic pressure. The exponential formulation for infarct stiffening proved both computationally efficient and physiologically grounded. Despite limitations, including spatial averaging and the absence of biochemical feedback, the modular nature of the model enables future integration with higher-order and mechanistic frameworks. Overall, this study demonstrates the importance of collagen turnover in shaping ventricular mechanics and provides a robust tool for exploring fibrotic remodeling processes in silico.

Bibliography

- World Health Organization. Cardiovascular diseases (cvds) fact sheet. [https://www.who.int/news-room/fact-sheets/detail/cardiovascular-diseases-\(cvds\)](https://www.who.int/news-room/fact-sheets/detail/cardiovascular-diseases-(cvds)), 2021.
- Nader Salari, Fatemeh Morddarvanjoghi, Amir Abdolmaleki, Shabnam Rasoulpoor, Ali Asghar Khaleghi, Leila Afshar Hezarkhani, Shamarina Shohaimi, and Masoud Mohammadi. The global prevalence of myocardial infarction: a systematic review and meta-analysis. *BMC Cardiovascular Disorders*, 23(206), 2023. doi: 10.1186/s12872-023-03231-w.
- Colleen M. Witzenburg and Jeffrey W. Holmes. Biomechanics of myocardial ischemia and infarction. In Gerhard A. Holzapfel and Ray W. Ogden, editors, *Biomechanics: Trends in Modeling and Simulation*, volume 20 of *Studies in Mechanobiology, Tissue Engineering and Biomaterials*, pages 233–270. Springer International Publishing, 2017. ISBN 978-3-319-41473-7. doi: 10.1007/978-3-319-41473-1_6.
- Saray Chen and Smadar Cohen. Principles of cardiovascular tissue engineering. In *Tissue Engineering*, chapter 18, pages 629–646. Elsevier, 2023. ISBN 978-0-12-824459-3. doi: 10.1016/B978-0-12-824459-3.00018-4.
- Hossein Sharifi, Charles K. Mann, Alexis L. Rockward, Mohammad Mehri, Joy Mojumder, Lik-Chuan Lee, Kenneth S. Campbell, and Jonathan F. Wenk. Multiscale simulations of left ventricular growth and remodeling. *Biophysical Reviews*, 13(5):729–746, October 2021. ISSN 1867-2469. doi: 10.1007/s12551-021-00826-5.
- Blaise A. Caraballo, Michael R. Zile, Ryuichi Tanaka, and George 4th Cooper. Left ventricular hypertrophy due to volume overload versus pressure overload. *Am J Physiol*, 263(4 Pt 2):H1137–H1144, October 1992. ISSN 0002-9513. doi: 10.1152/ajpheart.1992.263.4.H1137.
- Jack P. M. Cleutjens, Monique J. A. Verluyten, Jos F. M. Smits, and Mat J. A. P. Daemen. Collagen remodeling after myocardial infarction in the rat heart. *The American Journal of Pathology*, 147(2):325–338, 1995.
- Yu-Fang Jin, Hai-Chao Han, Jamie Berger, Qiuxia Dai, and Merry L. Lindsey. Combining experimental and mathematical modeling to reveal mechanisms of macrophage-dependent left ventricular remodeling. *BMC Systems Biology*, 5(60), 2011. doi: 10.1186/1752-0509-5-60.
- Pablo Sáez, Estefanía Peña, Miguel Ángel Martínez, and Ellen Kuhl. Mathematical modeling of collagen turnover in biological tissue. *Journal of Mathematical Biology*, 67(6–7):1765–1793, 2013. doi: 10.1007/s00285-012-0613-y.
- Natalia A. Trayanova and Raimond Winslow. Whole-heart modeling. *Circulation Research*, 108(1):113–128, 2011. doi: 10.1161/CIRCRESAHA.110.223610.
- Steven A. Niederer, Joost Lumens, and Natalia A. Trayanova. Computational models in cardiology. *Nature Reviews Cardiology*, 16(2):100–111, February 2019. ISSN 1759-5010. doi: 10.1038/s41569-018-0104-y.
- Luca Rosalia, Caglar Ozturk, David Van Story, Markus A. Horvath, and Ellen T. Roche. Object-oriented lumped-parameter modeling of the cardiovascular system for physiological and pathophysiological conditions. *Advanced Theory and Simulations*, 4, 2021.
- Louis Garber, Seyedvahid Khodaei, and Zahra Keshavarz-Motamed. The critical role of lumped parameter models in patient-specific cardiovascular simulations. *Archives of Computational Methods in Engineering*, 29(5):2977–3000, 08 2022. ISSN 1886-1784. doi: 10.1007/s11831-021-09685-5.
- Yubing Shi, Patricia Lawford, and Rodney Hose. Review of zero-d and 1-d models of blood flow in the cardiovascular system. *BioMedical Engineering OnLine*, 10(1):33, 04 2011. ISSN 1475-925X. doi: 10.1186/1475-925X-10-33.
- Emanuele Rondanina and Peter H. M. Bovendeerd. Evaluation of stimulus-effect relations in left ventricular growth using a simple multiscale model. *Biomechanics and Modeling in Mechanobiology*, 19(1):263–273, 2020. doi: 10.1007/s10237-019-01209-2.
- Colleen M. Witzenburg and Jeffrey W. Holmes. Predicting the time course of ventricular dilation and thickening using a rapid compartmental model. *Journal of Cardiovascular Translational Research*, 11(2):109–122, April 2018. ISSN 1937-5395. doi: 10.1007/s12265-018-9793-1.
- Kyoko Yoshida, Andrew D. McCulloch, Jeffrey H. Omens, and Jeffrey W. Holmes. Predictions of hypertrophy and its regression in response to pressure overload. *Biomechanics and Modeling in Mechanobiology*, 19(3):1079–1089, 2020. ISSN 1617-7940. doi: 10.1007/s10237-019-01271-w.

18. Bodh I. Jugdutt, Mohammad I. Khan, S. Joanne Jugdutt, and Gordon E. Blinston. Effect of enalapril on ventricular remodeling and function during healing after anterior myocardial infarction in the dog. *Circulation*, 91(3):802–812, 1995. doi: 10.1161/01.CIR.91.3.802.
19. W. P. Santamore and D. Burkhoff. Hemodynamic consequences of ventricular interaction as assessed by model analysis. *American Journal of Physiology-Heart and Circulatory Physiology*, 260(1):H146–H157, 1991. doi: 10.1152/ajpheart.1991.260.1.H146. PMID: 1992793.
20. Kenji Sunagawa, W. Lowell Maughan, and Kiichi Sagawa. Effect of regional ischemia on the left ventricular end-systolic pressure-volume relationship of isolated canine hearts. *Circulation Research*, 52(2):170–178, 1983. doi: 10.1161/01.RES.52.2.170.
21. Roy C P Kerckhoffs, Jeffrey Omens, and Andrew D McCulloch. A single strain-based growth law predicts concentric and eccentric cardiac growth during pressure and volume overload. *Mech Res Commun*, 42:40–50, 2012. doi: 10.1016/j.mechrescom.2011.11.004.
22. Edward K. Rodriguez, Anne Hoger, and Andrew D. McCulloch. Stress-dependent finite growth in soft elastic tissues. *Journal of Biomechanics*, 27(4):455–467, 1994. ISSN 0021-9290. doi: [https://doi.org/10.1016/0021-9290\(94\)90021-3](https://doi.org/10.1016/0021-9290(94)90021-3).
23. M. J. D. Powell. An efficient method for finding the minimum of a function of several variables without calculating derivatives. *The Computer Journal*, 7(2):155–162, 1964. doi: 10.1093/comjnl/7.2.155.
24. Paavo Uusimaa, Juha Risteli, Matti Niemelä, Jarmo Lumme, Markku Ikäheimo, Antti Jounela, and Keijo Peuhkurinen. Collagen scar formation after acute myocardial infarction: Relationships to infarct size, left ventricular function, and coronary artery patency. *Circulation*, 96(8):2565–2572, 1997. doi: 10.1161/01.CIR.96.8.2565.
25. Mihaela Rusu, Katrin Hilse, Alexander Schuh, Lukas Martin, Ioana Slabu, Christian Stoppe, and Elisa A. Liehn. Biomechanical assessment of remote and postinfarction scar remodeling following myocardial infarction. *Scientific Reports*, 9:16744, 2019. doi: 10.1038/s41598-019-53351-7.
26. Bodh I. Jugdutt, Michael J. Joljart, and Mohammad I. Khan. Rate of collagen deposition during healing and ventricular remodeling after myocardial infarction in rat and dog models. *Circulation*, 94(1):94–101, 1996. doi: 10.1161/01.CIR.94.1.94.
27. Yoshitatsu Nagatomo, Blase A. Carabello, Masayoshi Hamawaki, Shintaro Nemoto, Takeshi Matsuo, and Paul J. McDermott. Translational mechanisms accelerate the rate of protein synthesis during canine pressure-overload hypertrophy. *American Journal of Physiology - Heart and Circulatory Physiology*, 277(6):H2176–H2184, 1999. doi: 10.1152/ajpheart.1999.277.6.H2176.

Appendices

A.1. List of Abbreviation

Abbreviation	Definition
0D	Zero-Dimensional
A	Exponential curvature coefficient in EDPVR
B	Exponential amplitude coefficient in EDPVR
b(t)	Time-varying passive stiffness parameter
b _{mult}	Maximum infarct stiffness multiplier
CRC	Compliance–Resistance–Compliance
CT	Collagen Turnover
CVD	Cardiovascular Disease
ECM	Extracellular Matrix
ED	End-Diastolic
EDP	End-Diastolic Pressure
EDPVR	End-Diastolic Pressure-Volume Relationship
ED Wall Thickness	End-Diastolic Wall Thickness
ESPVR	End-Systolic Pressure-Volume Relationship
e(t)	Time-varying elastance waveform
FE	Finite Element
F	Deformation gradient
F _g	Growth component of deformation gradient
F _e	Elastic component of deformation gradient
G&R	Growth and Remodeling
HF	Heart Failure
HR	Heart Rate
IS	Infarct Size
k	Stiffening rate constant in CT law
LV	Left Ventricle
MAP	Mean Arterial Pressure
MI	Myocardial Infarction
MSZ	Mean Standardized Z-score
MMP	Matrix Metalloproteinase
PIIINP	N-terminal propeptide of type III procollagen
PO	Pressure Overload
PV	Pressure-Volume
Q	Flow rate
R	Resistance
RV	Right Ventricle
SBV	Stressed Blood Volume
TGF-β1	Transforming Growth Factor Beta 1
TIMPs	Tissue Inhibitors of Metalloproteinases
TVE	Time-Varying Elastance
V(t)	Instantaneous Cavity Volume
V ₀	Unloaded volume (EDPVR offset)

A.2. Input Parameters

Symbol	Description	Value
C_{vp}	Pulmonary venous compliance (ml/mmHg)	3.0
C_{as}	Systemic arterial compliance (ml/mmHg)	1.02
C_{vs}	Systemic venous compliance (ml/mmHg)	17.0
C_{ap}	Pulmonary arterial compliance (ml/mmHg)	2.0
R_{vp}	Pulmonary venous resistance (mmHg·s/ml)	0.015
R_{cs}	Systemic characteristic resistance (mmHg·s/ml)	0.023
R_{vs}	Systemic venous resistance (mmHg·s/ml)	0.015
R_{cp}	Pulmonary characteristic resistance (mmHg·s/ml)	0.06
R_{ap}	Pulmonary arterial resistance (mmHg·s/ml)	0.3

Table A3. Circulatory system parameters used in the model, unchanged during acute overloading or growth. Retrieved via Witzenburg et al. (2018) (16).

Parameter	Control	Acute (MI)
V_0 (ml)		14.0
E (mmHg/ml)		10.6
SVR (mmHg·s/ml)	2.68	1.65
SBV (ml)	390	457
A (1/ml)		0.042
B (mmHg)		1.673
HR (beats/min)	111	149
IS_{acute} (%)	–	23.2

Table A4. Baseline and acute hemodynamic parameters for myocardial infarction simulations. All the parameters are tuned by Witzenburg et al. (2018) with Jugdutt et al. (1995) (18) experimental measurements. Exceptions are for HR and IS, which are directly reported by the experimental measurements. Retrieved via (16).

Parameter	MI Value
$E_{ff,0}$	0.636
$E_{rr,0}$	-0.041
f_f	31.0
$s_{l,50}$	0.215
$r_{f,positive}$	36.4
$s_{t,50,positive}$	0.097
$r_{f,negative}$	576.0
$s_{t,50,negative}$	0.034

Table A5. Strain-driven growth law parameters for the myocardial infarction simulation, extracted from Witzenburg et al. (2018) (16).

A.3. Geometry

A.3.1. Compartmental Parameters Scaling. To maintain pressure continuity between the infarcted and non-infarcted regions while accounting for differences in unloaded geometry, each compartment is assigned a fraction of the total unloaded volume V_0 , based on infarct size $IS\%$. The unloaded volumes for the healthy (h) and infarcted (i) compartments are computed as:

$$V_{0,h} = V_0 \cdot (1 - IS), \quad V_{0,i} = V_0 \cdot IS \quad (\text{A21})$$

To preserve the shape and slope of the PV relationships under this geometric partitioning, the parameters A and E are scaled inversely with respect to the new unloaded volume of each compartment. Specifically:

$$A_{h,i} = A \cdot \left(\frac{V_0}{V_{0,h,i}} \right), \quad E_{h,i} = E \cdot \left(\frac{V_0}{V_{0,h,i}} \right) \quad (\text{A22})$$

These adjustments ensure that both the ESPVR and EDPVR remain physiologically realistic and that regional differences are properly accounted for during growth and remodeling.

A.3.2. Thin-Walled Sphere Geometry and Mechanics.

The thin-walled spherical approximation is used to model the left ventricular chamber geometry. It enables analytical expressions for unloaded and loaded dimensions and for wall stress computation. Below are the governing equations used throughout the framework:

Unloaded Geometry.

$$r_0 = \left(\frac{3}{4\pi} \cdot V_0 \right)^{1/3} \quad (\text{A23})$$

$$h_0 = \left(r_0^3 + \frac{3V_{\text{wall}}}{4\pi} \right)^{1/3} - r_0 \quad (\text{A24})$$

Loaded Geometry.

$$r = \left(\frac{0.75 \cdot V}{\pi} \right)^{1/3} \quad (\text{A25})$$

$$h = \left(h_0^3 + 3h_0^2 r_0 + 3h_0 r_0^2 + r_0^3 \right)^{1/3} - r \quad (\text{A26})$$

Hoop Stress (Laplace Law).

$$\sigma_{\text{hoop}} = \frac{P \cdot r}{2h} \quad (\text{A27})$$

Where:

- V_0 : unloaded cavity volume
- V_{wall} : myocardial wall volume
- r_0, h_0 : unloaded cavity radius and thickness
- r, h : loaded cavity radius and thickness
- V : loaded cavity volume
- P : internal ventricular pressure

A.4. Z-Score Based Optimization for Stiffness Law Calibration

To identify the optimal parameters governing infarct stiffening in the collagen turnover (CT) law, we formulated an objective function based on the mean squared z-score (MSZ). This approach quantifies the deviation between model predictions and experimentally measured targets over a defined post-infarction timeline.

The stiffening law was parameterized by the rate constant k and the stiffness multiplier b_{mult} . The optimal values were determined by minimizing the total MSZ across a set of hemodynamic and geometric outputs.

Metric Definition. For each physiological variable i , the mean squared z-score was computed over $N = 7$ experimental time points: days 2, 7, 14, 21, 28, 35, and 42. The MSZ for each variable is defined as:

$$\text{MSZ}_i = \frac{1}{N} \sum_{j=1}^N \left(\frac{y_{ij}^{\text{model}} - \mu_{ij}^{\text{exp}}}{\sigma_{ij}^{\text{exp}}} \right)^2 \quad (\text{A28})$$

Where:

- y_{ij}^{model} : simulation output for variable i at time point j ,
- μ_{ij}^{exp} : corresponding experimental mean,
- σ_{ij}^{exp} : experimental standard deviation.

Total Model Score. The overall model error was computed as the average of the five variable-specific MSZs:

$$\text{MSZ}_{\text{total}} = \frac{1}{5} \sum_{i=1}^5 \text{MSZ}_i \quad (\text{A29})$$

The five physiological targets used in this calculation are:

1. Maximum LV volume (ml),
2. Minimum LV volume (ml),
3. End-diastolic pressure (EDP, mmHg),
4. Mean arterial pressure (MAP, mmHg),
5. Normalized end-diastolic wall thickness.

This z-score-based metric was used as the cost function during both the grid search and local optimization stages of the infarct stiffening calibration. MSZ values below 1 indicate that model predictions fall within one standard deviation of the experimental mean, serving as a practical threshold for validation.

A.5. Collagen Turnover: Alternative Sigmoidal Formulation

An alternative time-dependent formulation of infarct passive stiffness was considered to replicate the sigmoidal accumulation of collagen observed in large-animal models. The function is defined as:

$$b(t) = b_0 \left[(1 + \alpha)(1 - e^{-kt})^n \right] \quad (\text{A30})$$

Where $b(t)$ is the time-varying infarct stiffness, b_0 is the initial infarct stiffness at baseline ($t = 0$), α is the asymptotic scaling multiplier, k is the stiffening rate constant (which controls how fast stiffening happens), and n is the sigmoidal shape factor (which determines the steepness and inflection point of the curve).

A.6. Joint Optimization of V_0 and V_{wall} for Geometric Consistency

To investigate the early discrepancies reported at Day 1 of growth—particularly the abrupt drop in EDP and myocardial wall thickness ratio (h_{ED})—a grid-based optimization was performed to assess the compatibility of baseline input parameters.

This optimization aimed to identify whether the reported values for unloaded cavity volume V_0 , myocardial wall volume V_{wall} , and baseline strains $E_{\text{ff},0}$, $E_{\text{tr},0}$ were mutually consistent with the observed acute hemodynamics. The target values were taken directly from Witzenburg et al. (2018) (16) used in the growth simulation framework.

Objective. The goal was to find a pair (V_0, V_{wall}) that minimizes the error in reproducing three experimental targets:

- Baseline fiber strain $E_{\text{ff},0} = 0.636$
- Baseline radial strain $E_{\text{tr},0} = -0.041$

- Remote-to-control ED wall thickness ratio

$$h_{ED}/h_{ED,0} = 0.96$$

The unloaded and loaded geometries were computed using the thin-walled spherical assumption. From these, myocardial strains and ED thickness ratios were derived.

The error function to be minimized was defined as the weighted sum of absolute differences between computed and target values:

$$\text{Error}(V_0, V_{\text{wall}}) = |E_{\text{ff},0}^{\text{sim}} - E_{\text{ff},0}^{\text{target}}| + |E_{\text{rr},0}^{\text{sim}} - E_{\text{rr},0}^{\text{target}}| + |h_{\text{ED ratio}}^{\text{sim}} - 0.96| \quad (\text{A31})$$

Parameter Ranges. The following search ranges were explored:

- $V_0 \in [7, 21]$ mL ($\pm 50\%$ around the reported baseline value)
- $V_{\text{wall}} \in [100, 100000]$ mL (broad exploratory range)